

Electro-Deformation and Poration of Giant Vesicles Viewed with High Temporal Resolution

Karin A. Riske and Rumiana Dimova

Max Planck Institute of Colloids and Interfaces, 14476 Golm, Germany

ABSTRACT Fast digital imaging was used to study the deformation and poration of giant unilamellar vesicles subjected to electric pulses. For the first time the dynamics of response and relaxation of the membrane at micron-scale level is revealed at a time resolution of 30 μ s. Above a critical transmembrane potential the lipid bilayer ruptures. Formation of macropores (diameter $\sim 2 \mu$ m) with pore lifetime of ~ 10 ms has been detected. The pore lifetime has been interpreted as interplay between the pore edge tension and the membrane viscosity. The reported data, covering six decades of time, show the following regimes in the relaxation dynamics of the membrane. Tensed vesicles first relax to release the acquired stress due to stretching, $\sim 100 \mu$ s. In the case of poration, membrane resealing occurs with a characteristic time of ~ 10 ms. Finally, for vesicles with excess area an additional slow regime was observed, ~ 1 s, which we associate with relaxation of membrane curvature. Dimensional analysis can reasonably well explain the corresponding characteristic timescales. Being performed on cell-sized giant unilamellar vesicles, this study brings insight to cell electroporation. The latter is widely used for gene transfection and drug transport across the membrane where processes occurring at different timescales may influence the efficiency.

INTRODUCTION

The interaction of electric fields with lipid membranes and cells has been extensively studied in the last decades (Neumann et al., 1989; Chang et al., 1992). The phenomenon of electroporation is of particular interest, because of its vast use in cell biology and biotechnology (Kinosita and Tsong, 1977; Chang et al., 1992; Zimmermann and Neil, 1996). Strong electric pulses of short duration induce electric breakdown of the lipid bilayer when the critical transmembrane potential is reached. The membrane becomes permeable for a certain time, because of transient pores across the bilayer, allowing the influx/efflux of molecules. Thus, electroporation is often used to introduce molecules like proteins, foreign genes (plasmids), antibodies, drugs, etc., into cells. Several studies in this area have already been conducted in an attempt to optimize and model the influence of the parameters of the electric field, e.g., intensity and duration (Chang and Reese, 1990; Dimitrov and Sowers, 1990; Tekle et al., 1994; Moroz and Nelson, 1997; Isambert, 1998; Smith et al., 2004). Even though a lot is known about the phenomenology of cell electroporation, the mechanism of pore opening across the lipid matrix is still not fully understood. Many studies have been performed therefore on model lipid vesicles to gain knowledge on electroporation (Teissie and Tsong, 1981; Glaser et al., 1988; Kakorin et al., 2003). Experiments on giant vesicles made of lipids and polymers are of special relevance because their size is comparable to cells and allows for direct observation using optical microscopy (Zhelev and Needham, 1993; Sandre

et al., 1999; Tekle et al., 2001; Aranda-Espinoza et al., 2001).

In the presence of electric fields, lipid vesicles are deformed, because of the electric stress imposed on the lipid bilayer, given by the Maxwell stress tensor. This effect has been studied theoretically, both for alternating fields (Kummrow and Helfrich, 1991; Hyuga et al., 1993) and for square-wave pulses (Hyuga et al., 1991a,b), but few experiments have been performed so far. In particular, experiments on electrodeformation caused by electric pulses have been performed only with small vesicles (Neumann et al., 1998; Griese et al., 2002; Kakorin and Neumann, 2002) where the observation is indirect and membrane tension and curvature may play a significant role. The vesicle deformation has been detected using turbidity, absorbance, and conductivity measurements where microsecond resolution can be achieved. Microscopy observation of effects caused by electric pulses on giant vesicles is difficult because of the short duration of the pulse. A possible solution to this problem is to slow down the processes by using a highly viscous fluid, e.g., glycerin, as medium instead of water (Sandre et al., 1999). However, such an approach can set physically different limitations on the response dynamics of the membrane. In addition, it may lead to a change in the hydration of the lipid bilayer and correspondingly alter the membrane properties.

In this study we use a fast imaging digital camera to record phase-contrast microscopy images of giant lipid vesicles with a high temporal resolution, up to 30,000 frames per second (fps) (1 image every 33 μ s). In this setup no labeling whatsoever is necessary and the medium is water. Our aim is to enrich the knowledge of vesicle electrodeformation and electroporation by means of accessing vesicle dynamics on

Submitted July 26, 2004, and accepted for publication November 22, 2004.

Address reprint requests to Dr. R. Dimova, Max Planck Institute of Colloids and Interfaces, Am Mühlenberg 1, 14476 Golm, Germany. Tel.: 49-331-567-9615; Fax: 49-331-567-9612; E-mail: dimova@mpikg.mpg.de.

© 2005 by the Biophysical Society

0006-3495/05/02/1143/13 \$2.00

doi: 10.1529/biophysj.104.050310

a submillisecond timescale. This is the first study so far reporting data on the deformation and poration of giant unilamellar vesicles (GUVs) performed with such time resolution.

The shape deformation induced on lipid vesicles by square-wave pulses depends on the conductivity ratio between the inner and outer vesicle solution. In this article we study the deformation of egg-PC GUVs in the absence of added salt. Under such conditions, spherical vesicles assume a prolate shape as a response to the external field, with the long symmetry axis aligning parallel to the electric field. Other shapes (mainly cylindrical; see Riske et al., 2004a) were observed in the presence of salt in the outer medium, and will be the issue of a subsequent article. The dynamics of electrodeformation in this work is presented for pulses of varying strength/duration. The data are discussed in terms of vesicle tension and/or excess area. For strong enough pulses, electroporation was generally accompanied by formation of visible macropores in the micrometer size range. Pore formation time, lifetime, and radius were measured on different vesicles. The electrodeformation dynamics was largely influenced by macropore formation.

The article is organized as follows. First we consider the vesicle response to square-wave pulses both when macro-poration is and is not induced by the field. The degree of deformation is considered in terms of membrane tension. The relaxation dynamics shows the presence of three regimes that we associate with: i), area relaxation due to stretching; ii), pore closure; and iii), curvature relaxation. In Appendix A1 we estimate the relative area change and attempt to correlate it with the electrical tension induced by the pulse. In Appendix A2 we compare our data with existing theories (Hyuga et al., 1991a,b).

MATERIALS AND METHODS

Preparation of giant unilamellar vesicles

Giant unilamellar vesicles of L- α -phosphatidylcholine from egg yolk, i.e., egg-PC (Sigma, St. Louis, MO) were grown using the electroformation method, described in Angelova and Dimitrov (1986). Briefly, 12 μ l of a 2 mg/ml lipid chloroform solution were spread on the surfaces of two conductive glasses (coated with indium tin oxide). The latter were kept under vacuum for \sim 2 h to remove all traces of the organic solvent. The two glasses were placed with their conductive sides facing each other and separated by a 2 mm-thick Teflon frame to form a chamber that was sealed with silicon grease. The glass plates were connected to a function generator and an alternating current of 1 V with a 10 Hz frequency was applied. The chamber was filled with 0.2 M sucrose solution and the voltage was gradually increased to 2.5 V in 0.5 V steps every 20 min. Vesicles of average size 10 μ m and large polydispersity were observed after \sim 4 h. The vesicle solution was removed from the electrosweating chamber and diluted 40 times into a 0.2 M glucose solution. This created a sugar asymmetry between the interior and the exterior of the vesicles. The solution was placed in an observation chamber where the direct current (DC) pulses were applied. Due to the differences in density and refractive index between the sucrose and glucose solutions, the vesicles were stabilized by gravity at the bottom of the chamber and had better contrast when observed with phase contrast

microscopy. The osmolarities of the sucrose and glucose solutions were measured with a cryoscopic osmometer Osmomat 030 (Gonotec, Berlin, Germany) and carefully matched to avoid osmotic pressure effects. The conductivities of the sucrose and glucose solutions were measured with a conductivity meter SevenEasy (Mettler Toledo, Greifensee, Switzerland), and found to be 6 ± 1 and 4.5 ± 1 μ S/cm, respectively. This gives a conductivity ratio between the inside and the outside solution of \sim 1.3.

Optical microscopy

An inverted microscope Axiovert 135 (Zeiss, Jena, Germany) equipped with a 20 \times phase contrast objective was used to visualize the GUVs. A fast digital camera HG-100 K (Redlake, San Diego, CA) was mounted on the microscope and connected to a personal computer. Image sequences were acquired at 20,000 and 30,000 fps, with picture resolution of 2.75 pixels/ μ m and 1.68 pixels/ μ m, respectively. Sample illumination was achieved with a mercury lamp HBO W/2. Sample heating due to illumination was measured to be $<2^\circ$ C, thus not significantly changing the bilayer properties. The observation chamber, purchased from Eppendorf (Hamburg, Germany), consisted of a Teflon frame confined above and below by two glass plates through which observation was possible. A pair of parallel electrode wires (92 μ m in radius) was fixed at the lower glass at a distance of 475 ± 5 μ m. The vesicles stayed at the bottom of the chamber due to gravity. The spacing between the electrodes is important for defining the field strength at the location of a selected vesicle above the floor of the chamber. Assuming the electrodes are perfect cylinders, the distance between them at the bottom glass is 674 μ m. Because we cannot precisely define the exact location of the vesicle center of mass above the glass (it depends on the size of the vesicle; the latter might as well be raised upwards by the field) we use the nominal gap distance of 500 μ m between the electrodes, and account for an error of \sim 10% in the electric field strength. The chamber was connected to a Multiporator (Eppendorf), which generated square-wave DC pulses. The pulse strength and duration could be set in the range 5–300 V (0.1 ± 0.01 – 6 ± 0.6 kV/cm) and 5–300 μ s, respectively. Time zero was defined as one frame before visible vesicle deformation occurred. Because occasional drift of the vesicles with time was observed we assume that there was no adhesion to the glass surface.

SOME IMPORTANT EQUATIONS

Transmembrane potential and poration limit

Lipid bilayers are impermeable to ions. In the presence of an electric field, charges accumulate at the bilayer interface. Thus, a transmembrane potential, V_m , is created across the membrane. At time t the potential induced on a nonconductive membrane by a DC pulse is given by (Kinosita et al., 1988):

$$V_m = 1.5 R \cos \theta E (1 - e^{-t/\tau_{\text{charg}}}), \quad (1)$$

where R is the vesicle radius, E the applied electric field, θ is the angle between the electric field and the vesicle surface normal, and τ_{charg} is the membrane charging time, given by (Kinosita et al., 1988):

$$\tau_{\text{charg}} = R C_m [1/\lambda_{\text{in}} + 1/(2\lambda_{\text{out}})]. \quad (2)$$

C_m is the membrane capacitance, \sim 1 μ F/cm² for lipid membranes (Needham and Hochmuth, 1989; Cevc, 1993), and λ_{in} and λ_{out} are the conductivities of the internal and external vesicle solution, respectively. For the low

conductivity solutions used in this work and for a typical vesicle radius $R = 15 \mu\text{m}$, $\tau_{\text{charg}} \sim 450 \mu\text{s}$, which in all measurements was longer than the pulse duration (50–300 μs , the upper limit being set by the instrument). To decrease τ_{charg} , so that a stationary state of fully charged membrane is reached during the pulse, one can either study vesicles with smaller radius or increase the conductivity of the solutions. However, using smaller vesicles implies lower picture resolution, whereas presence of salt (i.e., increased conductivity) induces morphological deformations other than ellipsoidal (Riske et al., 2004a). Furthermore, eventual poration adds additional concern of uncontrollable change in the conductivity ratio as a result of leakage. Thus, in this work we do not report data where the full charging of the membrane is reached.

At a certain critical transmembrane potential, V_c , electroporation occurs. Equations 1 and 2 are valid only for a nonconductive membrane, i.e., for $V_m < V_c$. Above the electroporation threshold the membrane becomes conductive and permeable. V_m cannot be further increased and can even decrease due to transport of ions across the membrane (Kinosita et al., 1988; Hibino et al., 1991).

Electrotension

The electric field induces a perpendicular stress in the bilayer (compression), given by the Maxwell stress tensor. Because the bilayer is almost incompressible, this stress can be associated with an increase in membrane area. In other words, the electric field adds an extra tension (σ_{el}) to the vesicle, which is given in terms of V_m as (Abidor et al., 1979; Needham and Hochmuth, 1989):

$$\sigma_{\text{el}} = \varepsilon\varepsilon_0(h/2h_e^2)V_m^2, \quad (3)$$

where ε is the dielectric constant of the aqueous solution, ε_0 the vacuum permittivity, h is the total bilayer thickness, $h \sim 39 \text{ \AA}$, and h_e the dielectric thickness, $h_e \sim 28 \text{ \AA}$, both measured for lecithin bilayers (Simon and McIntosh, 1986).

Surface area and volume of prolate ellipsoids

When GUVs are exposed to electric pulses, elongation along or perpendicular to the field is induced, as theoretically predicted by Hyuga et al. (1991b). The deformation depends on the conductivity ratio between the inside and the outside vesicle solutions, which will be reported in a following article. When no salt is added, giant vesicles filled with sucrose and immersed in a glucose solution (the conductivity ratio, $\lambda_{\text{in}}/\lambda_{\text{out}}$, is ~ 1.3) always assume a prolate shape as a response to square-wave pulses, with their symmetry axis oriented parallel to the field. The degree of deformation can be quantified by the ratio a/b , where a and b are the semiaxes along and perpendicular to the field, respectively. The surface area, A , of a prolate ellipsoid is given by:

$$A = 2\pi b(b + a \arcsin(e)/e), \quad (4)$$

where the eccentricity, e , is defined as $e^2 = 1 - (b/a)^2$. Using the area of a sphere with the same volume $A_0 = 4\pi(ab^2)^{2/3}$, we introduce a reduced area, A/A_0 . The measured increase in the reduced area, α_{app} , is then expressed as:

$$\alpha_{\text{app}} = (A - A_0)/A_0 = 1/2(a/b)^{1/3}(b/a + \arcsin(e)/e) - 1. \quad (5)$$

As mentioned before, when the induced transmembrane potential V_m reaches the threshold value V_c square-wave pulses cause electroporation. It is important to consider the constraints that apply to the vesicle shape in this case. During poration the bilayer becomes conductive and permeable, and aqueous pores form across the membrane allowing for leakage of the enclosed vesicle volume. In this case there is no conservation of area and volume (i.e., Eqs. 4 and 5 are no longer valid) and the degree of deformation of a spherical vesicle can depend both on an increase in the reduced apparent area or a decrease in the volume. Below the electroporation limit, the lipid bilayer keeps its integrity, remains impermeable, and behaves like a dielectric insulator. No change in volume occurs during the deformation, which solely results in an increase in the apparent area. The latter can be related to smoothing out of thermal fluctuations, if excess area is available, and/or to membrane stretching.

RESULTS AND DISCUSSION

We applied square-wave pulses of different strengths and durations to egg-PC giant unilamellar vesicles to study vesicle electrodeformation and electroporation. To facilitate the characterization of the shape deformation, the vesicles chosen were either spherical (no visible thermal fluctuations) or quasispherical (detectable thermal fluctuations). In the former case, the membrane could have nonzero initial tension, $\sigma_0 > 0$, whereas in the latter case it is reasonable to assume that the membrane was tension-free, i.e., $\sigma_0 \sim 0$. Although σ_0 is an important parameter influencing the degree of the vesicle deformation, we are not yet able to measure it in this experimental setup.

It has been previously reported that V_c depends on σ_0 . For tension-free vesicles $V_c \sim 1.1 \text{ V}$, decreasing with tension (Needham and Hochmuth, 1989; $V_c \sim 1.1 \text{ V}$ was measured for 1-stearoyl, 2-oleoyl phosphatidylcholine (SOPC) and dioleoyl phosphatidylglycerol, and we assume that it is the same for egg-PC). Thus, the electroporation threshold V_c can be different for each particular vesicle chosen depending on the initial tension. In agreement with this expectation, we observe poration of deflated vesicles (with visibly undulating membrane) at $\sim 1.1 \text{ V}$, whereas nonfluctuating vesicles, as presented further, readily porate at weaker fields. It is interesting to mention here that large unilamellar vesicles (with typical diameter of 100 nm) were found to electroporate at field strength of 0.2 V (Teissie and Tsong, 1981),

consistent with the fact that these small vesicles are usually under tension.

A clear sign that electroporation in a studied vesicle had occurred was the detection of optically resolvable macropores with diameters in the range $0.5\text{--}5\ \mu\text{m}$ (pores of smaller size cannot be optically detected). Their visualization was possible because of efflux of the inner sucrose solution, which under phase contrast microscopy appears darker than the external glucose solution. Thus, leakage results in disruption of the bright halo around the vesicle. Further in the text, depending on this observation, we will refer to the vesicles as “macroporated” or “nonmacroporated”.

In the following section we consider the shape response of a vesicle to electric pulses. We start with a simply designed and straightforward experiment where a sequence of increasingly strong/long pulses is applied to one vesicle. To understand the vesicle deformation behavior we first discuss the influence of the membrane tension on the electroporation threshold, and afterwards, call the attention to the effect of macroporation on vesicle dynamics. Then we focus on the shape relaxation and the corresponding characteristic times. Finally, we present results on electroporation, macropore sizes, formation, and lifetime.

Sequence of pulses applied to one vesicle

We consider the deformation of one vesicle subjected to a sequence of pulses of varying field strength. The pulses were applied with increasing pulse duration, t_p , (t_p was varied between $50\ \mu\text{s}$ and $300\ \mu\text{s}$ in $50\text{-}\mu\text{s}$ steps) at a fixed electric field strength E of $1\ \text{kV/cm}$, $2\ \text{kV/cm}$, and $3\ \text{kV/cm}$, in this order. To characterize the field strength, we introduce an apparent membrane potential at the end of the pulse $V_p = V_m(t = t_p)$ as calculated from Eq. 1. The series of applied pulses included conditions both below and above the tense-free electroporation threshold, $V_c = 1.1\ \text{V}$. The results for one such sequence presented in terms of the deformation ratio a/b are shown in Fig. 1. Overall, maximum deformation is observed close to the end of the pulse, $t = t_p$, after which the vesicle relaxes back to the original spherical shape ($a/b = 1$). Vesicle snapshots at maximum deformation for $t_p = 150\ \mu\text{s}$ pulses are given for every field strength. The insets present the maximum aspect ratio attained, $(a/b)_{\text{max}}$, for each pulse duration.

Although unpretentious and simple, this experiment brings out a variety of counterintuitive and complex effects. A gradual increase in $(a/b)_{\text{max}}$ occurs with pulse duration for $E = 3\ \text{kV/cm}$ (Fig. 1 C, inset), but for $E = 1$ and $2\ \text{kV/cm}$ (insets of Fig. 1, A and B, respectively) this is not observed. The same discontinuity in the dependence of $(a/b)_{\text{max}}$ was seen on a number of spherical nonfluctuating (tense) vesicles. In attempt to understand the reason behind this behavior we consider the poration conditions in the presented measurements. Arrows in the insets of Fig. 1 indicate the position of the tense-free poration limit V_c . Stars

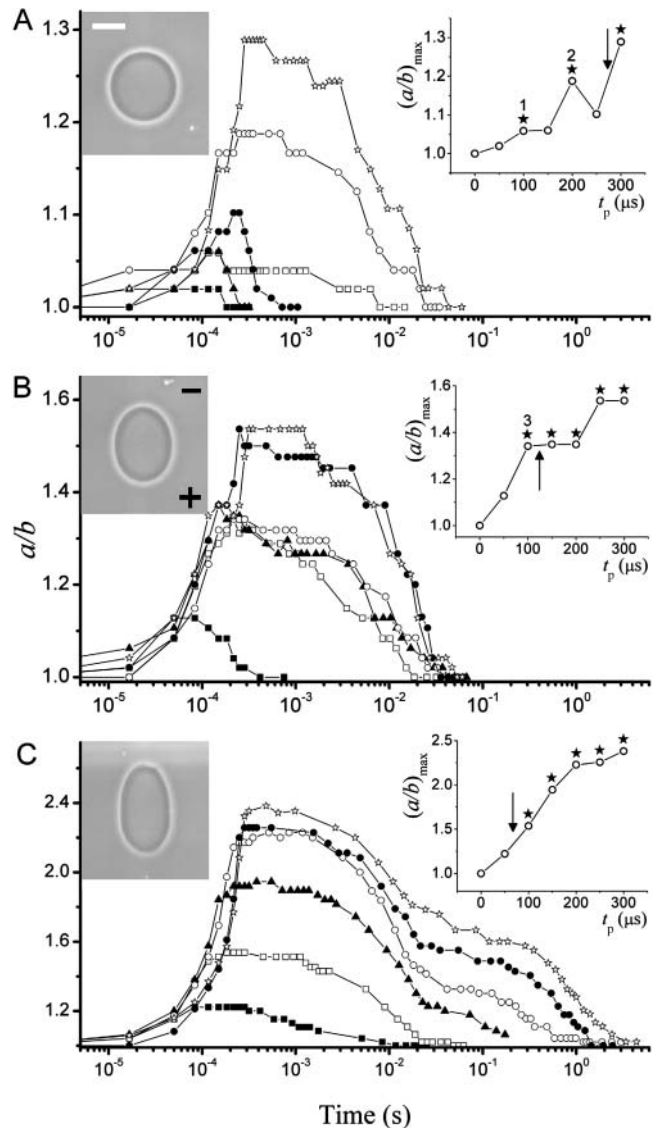


FIGURE 1 Degree of deformation (a/b) induced on one vesicle when applying different square-wave pulses: (A) $1\ \text{kV/cm}$, (B) $2\ \text{kV/cm}$, and (C) $3\ \text{kV/cm}$. For each pulse strength, the applied pulses were of duration $t_p = 50\ \mu\text{s}$ (\blacksquare), $100\ \mu\text{s}$ (\square), $150\ \mu\text{s}$ (\blacktriangle), $200\ \mu\text{s}$ (\circ), $250\ \mu\text{s}$ (\bullet), and $300\ \mu\text{s}$ (\star). The image acquisition rate was $30,000\ \text{fps}$. Time $t = 0$ was set as the beginning of the pulse. The insets show the maximum value of the deformation $(a/b)_{\text{max}}$ as a function of pulse duration, t_p , for each pulse strength. Arrows indicate the tense-free poration limit ($V_p > V_c$). The time interval between applying consecutive pulses was generally $5\ \text{min}$. The images on each graph correspond to the maximal elongation for the pulse of duration $t_p = 150\ \mu\text{s}$. The scale bar indicates $15\ \mu\text{m}$. The electrode's polarity is indicated with a plus and a minus sign on the second snapshot.

mark experiments for which macropores were observed. For all conditions above V_c macropores were detected as expected. However, in three subthreshold pulses ($V < V_c$), marked with numbers in the insets of Fig. 1, macroporation was also observed. Presumably, the vesicle has reached the poration limit because of some initial tension.

Apart from influencing $(ab)_{\max}$, macroporation affects the overall relaxation dynamics. When macroporated, the vesicle deforms more and relaxes more slowly compared to the cases of no macroporation (e.g., note the difference between the consecutive pulses $E = 1$ kV/cm, $t_p = 200$ and 250 μ s in Fig. 1 A, where the shorter pulse or weaker potential, *open circles*, which causes macroporation induces a stronger deformation than the longer pulse or stronger potential, *solid circles*, which does not induce macroporation).

The vesicle dynamics as presented in Fig. 1 is rich in complexity, and at first glance it looks insurmountable to disentangle all the phenomena influencing vesicle response to the applied pulses and relaxation. However, as we will find out, reconsidering the vesicle response in light of membrane tension and electroporation limits brings lucidity and understanding.

The deformation of a vesicle subjected to an electric pulse is caused by a compression force on the bilayer surface exerted by the Maxwell stress tensor. For an incompressible bilayer, this results in an increase in the membrane area. As discussed in the equation section, the effect is equivalent to applying an additional lateral tension, σ_{el} . The electrotension scales quadratically with the transmembrane potential (see Eq. 3). The dependence was earlier explored by Needham and Hochmuth (1989) who studied electroporation of giant lipid vesicles (later repeated on polymer vesicles by Aranda-Espinoza et al., 2001). The membrane tension before applying the electric field was maintained/measured with micropipettes. The overall membrane tension, σ , was presented as a sum of the electrotension, σ_{el} , and some initial tension applied by the pipettes, σ_o . The authors observed that electroporation (i.e., lysis) occurred when the relative increase in the area, α , (defined as the area difference relative to a tension-free membrane) reached a certain threshold value or when the total tension of the membrane amounted to the critical tension, σ_c . The total membrane tension, σ , was presented as linearly proportional to the relative area increase, α , with the proportionality factor being the membrane stretching elasticity coefficient, K (for egg-PC, $K \sim 140$ dyn/cm; Needham, 1995): $\sigma = K\alpha$. It is important to note that in our measurements we can only access α_{app} (Eq. 5), which does not necessarily correspond to the relative area increase, α , as measured in experiments with micropipettes (see, e.g., Evans and Rawicz, 1990). Note that α_{app} and α are defined as area changes relative to two different areas: the initial projected vesicle area and the area of the tension-free vesicle, respectively. In our experiments the area at zero tension is, in general, not accessible and can vary from pulse to pulse. In the Appendix A1 we give examples for the behavior of α_{app} obtained from our measurements and an attempt to correlate it with the applied σ_{el} .

Literature data about the critical value of the relative area increase vary between 3% (Needham and Hochmuth, 1989) and 5% (Rawicz et al., 2000), both measured with micropipettes. Presumably, our experimental data should be closer

to the value of Needham and Hochmuth (1989) because in their work lysis was caused by electric pulses, whereas in Rawicz et al. (2000) the rupture tension was reached only by an increase in the micropipette suction pressure. The lysis tension as given by Needham and Hochmuth (1989) is $\sigma_c \approx 5.7$ dyn/cm for SOPC vesicles. Evans et al. (2003) report an increase in the membrane strength (i.e., increase in the breakdown tension σ_c) when the tension loading rate is raised. In their work, vesicles were ruptured with a steady ramp of micropipette suction pressure. In our experiment, as well as in Needham and Hochmuth (1989), the tension loading rate was not constant. The tension, as defined by Eqs. 3 and 1, changes during the pulse when the membrane is gradually charged, and exhibits a complex dependence on time (see Eq. 6 in Appendix A1) and, respectively, the loading rate is not constant but varies with time. Actually, the loading rate does not seem to affect σ_c when tension is induced by electric pulses: for stronger fields where σ_{el} is >5.7 dyn/cm vesicles do rupture. Thus, the results in this work, as in Needham and Hochmuth (1989), can be discussed without considering changes in the membrane rupture limit due to different loading rates.

In light of the concept that V_c depends on the initial membrane tension (Needham and Hochmuth, 1989), we consider again the results presented in Fig. 1 in an attempt to understand the discontinuity observed in $(ab)_{\max}$ (insets). The three pulses indicated with numbers in the insets of Fig. 1, A and B, are cases of subthreshold macroporation ($V_p < V_c$). Presumably the membrane rupture is a consequence of some initial (preceding the pulse) tension. Because no thermal fluctuations were observed in the beginning of the pulse sequence, this vesicle could have indeed started with some initial tension σ_o . For these three cases of macroporation at $V_p < V_c$ one can estimate the minimum value of σ_o from the difference $\sigma_c - \sigma_{el}$ (the electrotension $\sigma_{el}(V_p)$ is calculated using Eq. 3). The total tension would then be $\sigma = \sigma_o + \sigma_{el}$. Fig. 2 presents tension isolines for various σ_o . If $\sigma_o = 0$, $\sigma = \sigma_{el}$, and one can position the experimental condition points (*circles* and *stars*) on the tension-free isoline as a function of the applied transmembrane potential V_p . Of these data points, the stars indicate the cases of poration $\sigma = \sigma_c$ (the numbers correspond to those indicated in the insets in Fig. 1). Obviously, these points could not have been lying on this isoline because the vesicle porated. Shifting the points upwards to reach σ_c (*dashed arrows*) one can locate the isoline of minimum σ_o , which the vesicle must have had before the pulse was applied (the corresponding σ_o -isolines are displayed in Fig. 2). The numbers on the graph indicate the sequence in which the pulses were applied. One notices that the estimated minimum σ_o decreases with every following pulse (the vesicle relocates on a lower σ_o -isoline). This is understandable because after the formation of macropores, the vesicle volume decreases due to efflux of internal solution, whereas its area remains constant (if the pore resealing process is not defective). Thus, a decrease in

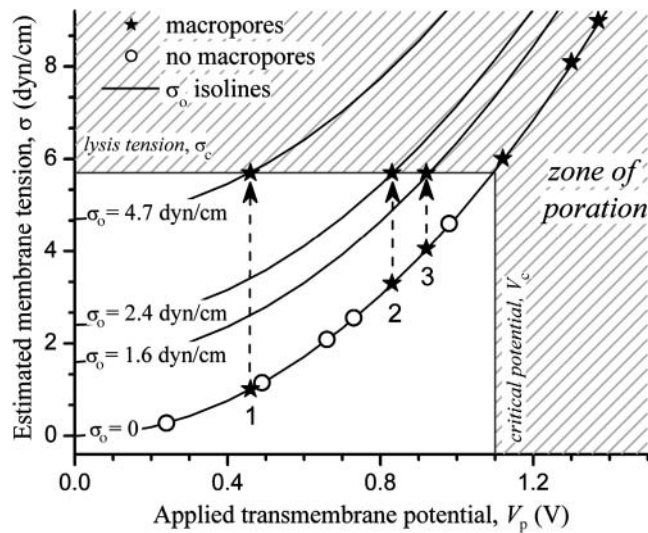


FIGURE 2 Total membrane tension σ , as a function of the transmembrane potential at the end of the pulse, V_p (σ is given by $\sigma = \sigma_{el} + \sigma_0$, where the electotension σ_{el} was calculated from Eq. 3 and σ_0 is some initial tension). Cases where no macroporation was observed are displayed as open circles (\circ), whereas those where macropores were visualized are indicated with stars (\star). The shaded area indicates zone of expected poration where V_p is above the tense-free critical potential, $V_c = 1.1$ V, and/or the membrane tension is above the critical rupture tension $\sigma_c = 5.7$ dyn/cm. On three occasions (marked with numbers according to the sequence of the applied pulses) the vesicle macroporated below the poration limit ($V_p < V_c$), presumably because of some initial membrane tension, σ_0 . Isolines at different σ_0 present possible trajectories or states of the vesicle for the three cases where macroporation was observed at $V_p < V_c$.

σ_0 along the pulse series is, indeed, to be expected. Furthermore, visible thermal fluctuations were detected after the pulse $E = 3$ kV/cm, $t_p = 150$ μ s, indicating that σ_0 has reached 0 by then. The appearance of macropores during a pulse could cause a decrease of up to 4% in volume. The total decrease in vesicle volume by the end of the whole pulse sequence was $\sim 30\%$.

Having understood the observed fluctuations in the maximum vesicle deformation α_{app} with regards to poration, we now address the overall vesicle dynamics, i.e., the shape of the curves in Fig. 1.

Relaxation dynamics

We consider in details two typical deformation dynamics of vesicles below ($E = 1$ kV/cm, $t_p = 250$ μ s from Fig. 1 A) and above ($E = 3$ kV/cm, $t_p = 100$ μ s from Fig. 1 C) the electroporation limit. These two cases are presented in Fig. 3, A and B, respectively. Snapshots of the vesicle at different times indicated on the graph are also shown above and below the figure. Macropores, as indicated on one vesicle snapshot with arrows, were only detected for the conditions shown in Fig. 3 B. They are located close to the vesicle poles. This observation is consistent with Eq. 1, which shows that the membrane potential is maximal at the vesicle poles (see also

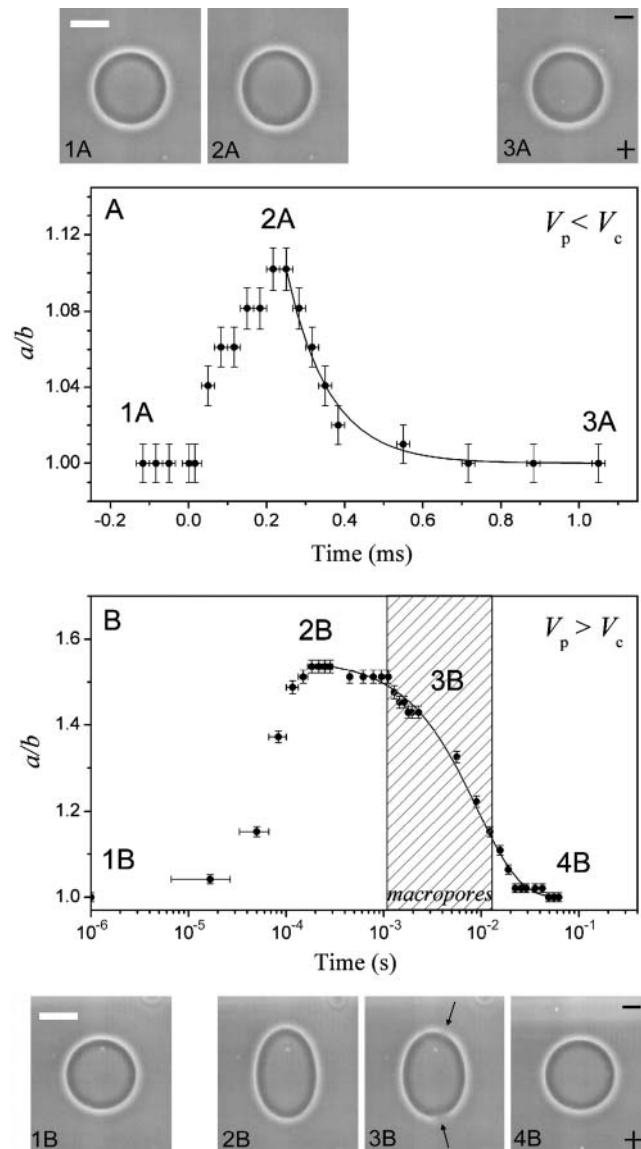


FIGURE 3 Degree of deformation (a/b) attained by one vesicle when subjected to two different square-wave pulses: (A) $E = 1$ kV/cm, $t_p = 250$ μ s ($V_p < V_c$); and (B) $E = 3$ kV/cm, $t_p = 100$ μ s ($V_p > V_c$). Time $t = 0$ was set as the beginning of the pulse. The image acquisition rate was 30,000 fps. Snapshots corresponding to the time frames indicated with numbers on the graphs are shown above and below the graphs. The scale bar on the first snapshots in the series corresponds to 15 μ m. The electrode's polarity is indicated with a plus and a minus sign on the last snapshots. The shaded area in panel B shows the time interval when macropores were detected (indicated with arrows on snapshot 3B). Note that the time in panel B is given in logarithmic scale. Solid lines indicate exponential fit with decay times (A) τ_1 and (B) τ_2 (see text for details).

Kinosita et al., 1988 and Hibino et al., 1991). The maximum deformation achieved in the case of macroporation is much higher than the one observed in the absence of poration, not only because of the different pulse strength/duration, but also because the vesicle no longer deforms as an object of closed surface and because there is extra area contributed by the

macropores. One cannot directly compare a/b displayed on Fig. 3, *A* and *B*, because the degree of deformation may depend on initial vesicle conditions, such as tension and/or excess area. After the electric pulse is switched off, the vesicle relaxes back to a sphere, i.e., a/b decreases back to 1.

The relaxation of the deformation acquired is also very different for the macroporated and for the nonmacroporated case, as one can easily judge by eye (note the difference in the x axis scale in Fig. 3, *A* (linear) and *B* (logarithmic)). Both relaxation processes could be fitted to single exponential decays (Fig. 3, *solid lines*). A fast characteristic time $\tau_1 = 110 \mu\text{s}$ is achieved for the relaxation of the nonmacroporated case (Fig. 3 *A*), whereas an almost one order of magnitude longer decay time $\tau_2 = 9.2 \text{ ms}$ is obtained for the macroporated case (Fig. 3 *B*). Further in the text we will refer to τ_1 and τ_2 as the characteristic relaxation times for nonmacroporated and macroporated vesicles, respectively. Statistics and data from different vesicles will be given below as well as deeper analysis and interpretation of the relaxation times.

An interesting characteristic of the relaxation curves in case of macroporation is the apparent delay time after the end of the pulse (between $150 \mu\text{s}$ and 1 ms ; see also Fig. 1) before the relaxation commences. This plateau-like feature is enhanced by the logarithmic-axis presentation and by the pixel resolution (see the stepwise decrease in Fig. 1 *B*). However, as will be discussed in Appendix A2, the appearance of a ‘‘plateau’’ can be due to inertial effects in the vesicle response.

Apart from the two decay times mentioned above, τ_1 being the one for nonmacroporated vesicles and τ_2 for macroporated ones, we observe a third characteristic time τ_3 in the relaxation dynamics (see Fig. 1 *C*, $E = 3 \text{ kV/cm}$, $t_p = 150\text{--}300 \mu\text{s}$). This coincides with detection of thermal fluctuations, which significantly increase after each of these pulses. The relaxation dynamics was analyzed for different vesicles subjected to pulses of different strengths/durations. The decay times from the exponential fits always fall in one of the three categories (τ_1 , τ_2 , or τ_3), depending on whether the vesicles showed detectable macropores and/or thermal fluctuations. The results obtained for τ_1 , τ_2 , and τ_3 are presented in Fig. 4 *A* as a function of V_p . The decay times found for nonmacroporated vesicles are all $0.1 \text{ ms} \leq \tau_1 \leq 0.5 \text{ ms}$. Among the different vesicles, τ_1 does not correlate with V_p because of the different initial tension of the membranes. In some macroporated vesicles τ_1 is also detectable, but in most of the cases it cannot be clearly distinguished from τ_2 . Thus, in experiments (where the third relaxation process was not observed) the data could be fitted to a single exponential (τ_2). This is understandable because the rate-limiting step is always the slower of two processes ($\tau_2 > \tau_1$).

In the following paragraphs we attempt to discern the processes defining the characteristic times involved in the vesicle relaxation. We use the concept of dimensional

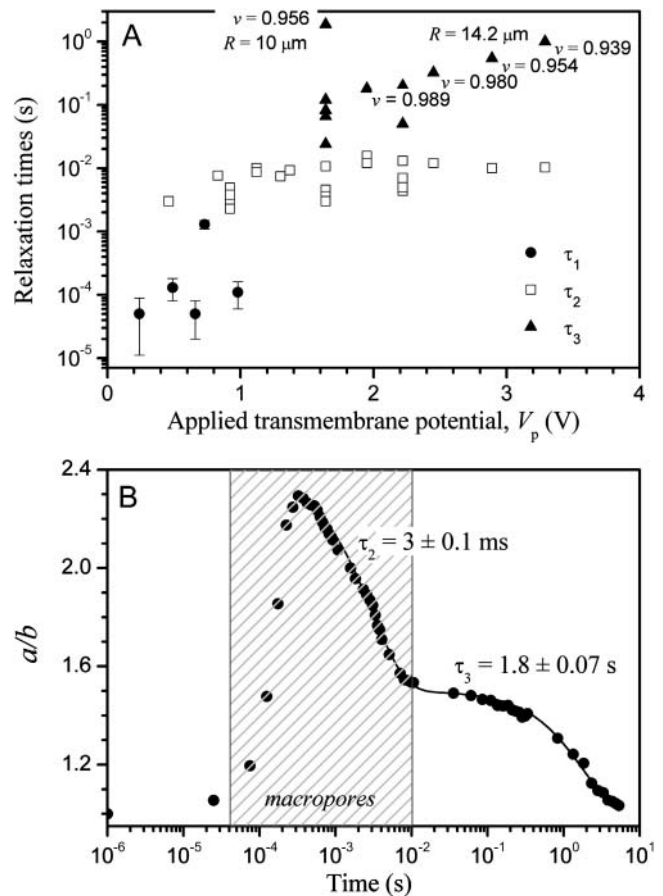


FIGURE 4 (A) Decay times obtained from exponential fits to the relaxation of a/b with time as a function of the apparent transmembrane potential V_p at the end of each pulse. The relaxation times are divided in three categories: without macropores, τ_1 (●), and with macropores, τ_2 (□) and τ_3 (▲). As discussed in the text, τ_3 is associated with membrane fluctuations and depends on the reduced volume of the vesicles, v , (for clarity, the values of v are indicated on the figure only in some of the cases). (B) Response and relaxation of a macroporated vesicle ($E = 2 \text{ kV/cm}$, $t_p = 200 \mu\text{s}$, $t = 0$ was set as the beginning of the pulse) and corresponding exponential fits with decay times τ_2 and τ_3 as described in the text. The image acquisition rate was 50,000 fps. The shaded area indicates the time interval when macropores are detected. The radius of this vesicle is $10.8 \mu\text{m}$.

analysis to distinguish the main physical parameters influencing the vesicle behavior in the three different regimes. Intuitively, one would relate τ_1 to the relaxation of the total membrane tension achieved at the end of the pulse, which is the sum of the electrotension σ_{el} and the initial tension σ_o . As discussed above, the total tension of the vesicles observed at maximum deformation is in the stretching regime of the membrane. Thus, τ_1 relates mainly to the relaxation of membrane stretching: $\tau_1 \sim \eta_s/\sigma$, where η_s is the surface viscosity of the bilayer (the surface viscosity of a membrane has units (bulk viscosity) \times (membrane thickness), i.e., dyn s/cm). The shear surface viscosity of the membrane is $\sim 3 \times 10^{-6} \text{ dyn s/cm}$ (Dimova et al., 1999) corresponding to values reported for the diffusion constant of

molecular probes in lipid bilayers $D \approx 10^{-13} - 10^{-12}$ m²/s (Orädd et al., 1994). Some other measurements of the surface viscosity (Sandre et al., 1999, later interpreted by Brochard-Wyart et al., 2000) determined by following the dynamics of macropores on giant vesicles suggest a value for η_s , which is two orders of magnitude higher: $\eta_s \approx 3.5 \times 10^{-4}$ dyn s/cm as given in Brochard-Wyart et al. (2000). (This value is somewhat different from the original value reported by the same group where $\eta_s \approx 5 \times 10^{-3}$ dyn s/cm, Sandre et al., 1999, but we suppose that the interpretation in the later article is more accurate.) This is probably because the reported experiments are related to dilation rather than to shearing the membrane. We chose to work with this dilatational (and not the shear) surface viscosity (i.e., we use the value given by Brochard-Wyart et al., 2000) because it is the more relevant for the experimental conditions in our study. Coming back to τ_1 , for membrane tensions of the order of 5 dyn/cm (which should be around the maximum tension before the membrane ruptures) one obtains $\tau_1 \sim \eta_s/\sigma \sim 100$ μ s, which is very close to the value experimentally measured by us.

The decay time of macroporated vesicles, τ_2 , shows a quite narrow distribution among different vesicles subjected to pulses of different strengths: 7 ± 4 ms (see Fig. 4 A). We observe that this relaxation process takes place during the time interval when pores are present. This is illustrated in Fig. 4 B where the relaxation dynamics of a macroporated vesicle is presented. The time interval, in which a macropore is observed, τ_{pore} , is indicated. Because of the clear correlation between τ_{pore} and τ_2 we assume that the dynamics is determined by the closing of the pores. The driving force for the process of pore closure is the line tension that originates from the energetic cost to rearrange or curve the lipid molecules on the edge of the pore. Thus, the characteristic time should be defined as $\tau_2 \sim \eta_s r_{\text{pore}}/(2\gamma)$, where r_{pore} is the pore radius and γ is the line energy per unit length ($\gamma \sim \kappa/2h$ where κ is the bending stiffness of the bilayer and h is the membrane thickness ~ 4 nm), which is of the order of 10^{-6} dyn (10^{-11} J/m; Harbich and Helfrich, 1979). For a typical pore radius of 1 μ m we obtain $\tau_2 \sim 10$ ms. Of course, the presence of smaller pores (but still in the micron-size range) in the membrane should decrease τ_2 and accelerate the relaxation dynamics. Nanometer-size pores, which cannot be detected optically, may also be present as demonstrated by electroporation experiments on planar lipid bilayers (Chernomordik et al., 1987). These membranes, however, are connected to a reservoir of material (the meniscus) that can influence the redistribution of molecules and affect the resealing process (see, e.g., Weaver and Chizmadzhev, 1996) leading to long lifetime of the pores (on the order of seconds or even minutes).

We recall here that the pore opening/closing dynamics in our work is resolved by observation of the flux of sucrose leaving the vesicle. An obvious question arises whether the relaxation is related to the leakage rather than to the

pore closure. We therefore compare the leakage time with the pore opening time. The efflux decreases the vesicle volume, i.e., increases the excess area and releases the membrane tension. Then the leakage time should be of the order of $\eta R^2/(\sigma r_{\text{pore}})$ (Sandre et al., 1999), where η is the sucrose solution viscosity (at the glucose/sucrose concentrations in our experiments η is between 1.1 and 1.2×10^{-2} poise). For r_{pore} around 1 μ m we obtain a value of the order of 0.01–0.1 ms (depending on the final tension), which eliminates the hypothesis that the relaxation described by τ_2 is limited by the efflux of sucrose. In the discussion above we assumed that the leakage is mainly determined by the viscosity of the solution and not of the surface membrane viscosity (fast leak-out regime; see, e.g., Brochard-Wyart et al., 2000).

The additional time τ_3 is detected when pulses are applied to vesicles with excess surface area or to vesicles that gain excess area during the macroporation. The excess area available for shape changes can be characterized by a dimensionless volume-to-area ratio $\nu = (3V/4\pi)(4\pi/A)^{3/2}$ where V is the vesicle volume, $V = (4\pi/3)ab^2$. This reduced volume ν is 1 when the vesicle is a sphere and smaller than 1 in the rest of the cases. As one can expect, vesicles with small reduced volumes, i.e., large excess area, will deform more when the field is applied. Vesicles that showed very little thermal fluctuation (with ν close to 1) had $\tau_3 \sim 0.1$ s, whereas τ_3 increased up to 3 s in strongly fluctuating vesicles (the lowest value of ν for this relaxation regime was ~ 0.9). We interpret this relaxation as associated with the process of displacing the volume, ΔV , of fluid involved in the elliptical vesicle deformation, $V_{\text{el}} = 4\pi R^3/(3\nu)$, compared to a relaxed spherical shape, $V_{\text{sph}} = 4\pi R^3/3$. The restoring force is related to the bending elasticity of the lipid bilayer. The decay time can be presented as $\tau_3 \sim \eta \Delta V/\kappa$, with $\Delta V = V_{\text{el}} - V_{\text{sph}} = 4\pi R^3/(3\nu) - (4/3)\pi R^3$, leading to $\tau_3 \approx (4\pi\eta R^3/3\kappa)(1/\nu - 1)$, where η is the bulk viscosity of sucrose/glucose solution, as above, and κ is the bending elasticity modulus of the membrane. For egg-PC $\kappa \approx 10^{-12}$ erg (Mutz and Helfrich, 1990; Schneider et al., 1984). Thus, for ν varying between 0.99 and 0.94 (which is the interval of reduced volumes within which τ_3 is detected) we obtain τ_3 between ~ 0.5 and 3 s, which corresponds excellently to the measured data: vesicles of the same size have longer relaxation times when their reduced volumes are small (see data for τ_3 in Fig. 4 A and the indicated values for ν). The example in Fig. 4 B is for a vesicle of $\nu = 0.956$.

We recall here that all of the three decay times have been deduced from the relaxation dynamics of the dimensionless length a/b . The corresponding characteristic times for the vesicle area or volume could differ by a factor of 2 or 3, respectively, accounting for the dimensionality of each of these parameters.

The overall behavior of a/b with time (steep increase, delay time at maximum, exponential decrease) resembles the theoretical prediction in Hyuga et al. (1991a,b). However, no

reasonable quantitative agreement could be obtained when the pulse strength/duration was varied. In their model, no area stretching is taken into account, and the only elastic property entering into their theory is the bending energy (see the Appendix A2).

Macropores

Strong pulses above the electroporation threshold, or pulses that bring the membrane above the lysis tension, induce the formation of macropores in giant vesicles. The macropores are located close to the vesicle poles, where the transmembrane potential V_m is maximal (see Eq. 1). A macropore is visualized by the efflux of the darker sucrose solution from the vesicle interior through the pore, as shown for one vesicle in Fig. 5. In this example ($E = 2$ kV/cm, $t_p = 200$ μ s), the efflux of sucrose was first detected at 125 ± 25 μ s. For these parameters of the field (pulse strength/duration) if the starting tension of the membrane is negligible, the critical voltage, V_c , should be reached in 130 μ s. Three macropores are distinguished facing the negative electrode, with diameters $d_{\text{pore}} \sim 2.5$ μ m. Macropores facing the positive electrode are also seen, although they are not as easily distinguishable as the ones on the top. In general, the location of the pores (whether facing the positive or the negative electrode) on various vesicles was not observed to be dependent on the field direction. The lifetime τ_{pore} of all macropores was ~ 10 ms.

The maximal macropore sizes (d_{pore}), formation times (t_{pore}), and lifetimes (τ_{pore}) were measured for >15 different vesicles, with some vesicles rupturing with several macropores. Among the different vesicles, the macropore formation time found (the time interval in which pores were detected) was usually $t_{\text{pore}} = 175 \pm 20$ μ s. In some cases a delay of up to 1 ms was observed. However, we can only visualize macropores that are situated on the vesicle cross section located at the focal plane of the microscope objective. Thus, “invisible” macropores that could have been out of the focal plane were not detected. In addition, we are not able to distinguish one big macropore from few neighboring macropores.

Because the initial tension of the vesicle cannot be measured in this setup, we cannot predict at what time a vesicle would reach V_c . We only measure the lifetime of the macropore, τ_{pore} , which is shown in Fig. 6 as a function of their maximum diameter d_{pore} . Despite the significant

imprecision in the estimation of both τ_{pore} and d_{pore} due to the image resolution, an overall increase of τ_{pore} with d_{pore} is detected. On the average, τ_{pore} increased from 4 to 17 ms as d_{pore} increased from 1 to 4 μ m. The lifetime of the pore includes a very short period of exponential growth of the pore (~ 0.4 ms, see Fig. 4 B) and a much longer time in which the pore closes at a constant velocity of $\gamma/(2\eta_s)$ (Sandre et al., 1999). Then ($\tau_{\text{pore}} - 0.4$) ms is essentially the time by which the pore radius decreases by $d_{\text{pore}}/2$, i.e., $\tau_{\text{pore}} = 0.4$ ms + $d_{\text{pore}}\eta_s/\gamma$, which is presented with the dashed line in Fig. 6.

Some macropores, however, fell completely out of this trend, and had much longer lifetime, between 50 and 130 ms (note the y axis break in Fig. 6). These macropores were detected in vesicles that appeared to be under tension (no fluctuations) and subject to weak pulses, e.g., $E = 1$ kV/cm, $t_p = 100, 200,$ and 300 μ s. We suspect that after the pulse is applied, the pore opens, and the tension is only partially relieved. The residual tension balances the line energy and thus stabilizes the pore. In a similar way, Zhelev and Needham (1993) showed that macropores could be stabilized for almost a second, when a certain tension was applied to a vesicle. Because of the compound composition of the membrane (egg-PC is a mixture of phosphatidylcholine lipids of different acyl chains) one may speculate that the line tension of pores in such membranes may be lowered due to the rearrangement of “more suitable” molecules at the pore rim. This presumably leads to longer pore lifetimes, which is consistent with studies on erythrocyte membranes where a long-lasting permeabilized state was reported (Sowers, 1986). Indeed, in preliminary experiments on two-component lipid mixtures of dioleoylphosphatidylcholine and a small fraction of dioleoylphosphatidylglycerol we observed much longer pore lifetimes of the order of 1 s (data not shown). In this case the phosphatidylglycerol presumably acts as pore stabilizer (Riske et al., 2004b) reducing the edge energy. In the case of pure egg-PC, however, the lowering of the line tension should affect the lifetime of all pores (see Fig. 6) and should reflect in similar scatter in the data for the relaxation time τ_2 , which was not observed.

Apart from the line tension, the shear surface viscosity of the membrane also influences the lifetime of the pores. Some preliminary experiments performed on polymersomes (i.e., membranes made of diblock copolymers, see, e.g., Discher et al., 1999) showed much longer pore lifetime — of the

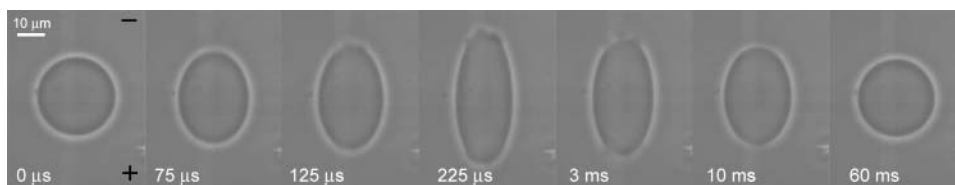


FIGURE 5 A snapshot sequence of a vesicle subjected to a pulse, $E = 2$ kV/cm, $t_p = 200$ μ s. The image acquisition rate was 50,000 fps. Macropores are first visualized in the third frame ($t = 125$ μ s). The electrode's polarity is indicated with a plus (+) and a minus (−) sign on the first snapshot.

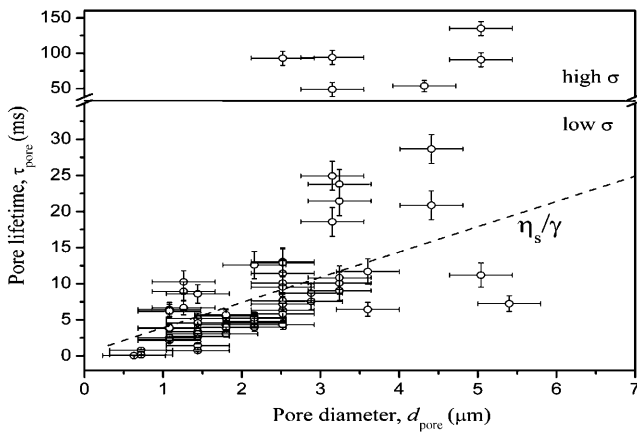


FIGURE 6 Macropore lifetime (τ_{pore}) as a function of pore diameter (d_{pore}) measured on 15 different vesicles. The dashed line has a slope η_s/γ (see text for details). The horizontal line delimits a region of pores with longer lifetime. Presumably they have been stabilized by high residual membrane tension, σ , after applying the pulse (note the difference in the axes).

order of a second (data not shown). These polymer membranes have extremely slow response and are characterized by surface viscosity, which is ~ 500 times higher than that of lipid membranes (Dimova et al., 2002). Correspondingly, the observed pore lifetimes were ~ 2 orders of magnitude longer (~ 1 s) in agreement with recent experiments reported by Bermúdez et al. (2003).

PERSPECTIVES

The reported results on the deformation and relaxation of giant unilamellar vesicles are the first to show the shape response of a giant lipid vesicle to an electric pulse at high time resolution. The presented data cover six decades of time. The response of the system depends entirely on the membrane properties (stretching and bending elasticity, surface viscosity, edge energy) and on the media viscosity. Having described the behavior of the pure model system (pure lipid vesicles in salt-free solutions), a natural continuation of this work is to advance to more biologically relevant conditions for understanding electrodeformation and electroporation processes in cells. We now direct our attention toward studying the influence of additives both in the bulk solution (e.g., salt) and in the membrane. The conductivities of the external and internal vesicle solutions play significant roles in two ways: i), The salt asymmetry on

both sides of the vesicle membrane defines the morphological deformation. Depending on the conductivity ratio of the two solutions the vesicle can assume the shape of a prolate or oblate ellipsoid, or even a cylinder as already observed in some preliminary experiments (Riske et al., 2004a). ii), The ionic strength of the solution effectively alters the field strength. The poration and the lifetime of the pores, on the other hand, do not depend on the composition of the solvent but rather on additives in the lipid bilayer (Saitoh et al., 1998; Karatekin et al., 2003). Molecules of various geometries, when incorporated in the membrane, may dramatically vary the line tension (Chernomordik et al., 1985). As briefly mentioned above, preliminary experiments (data not shown) show that additives like dioleoylphosphatidylglycerol drastically increase the pore lifetime.

Electroporation is important not only in terms of making the membrane permeable to molecules across the bilayer. It is indispensable for electrofusion, being essentially its precursor (Sowers, 1986; Ramos and Teissié, 2000). The opening of pores on two opposing membranes is the necessary condition for the bilayers to fuse. Fast digital imaging can then bring significant insight into the opening of fusion pores and the expanding of the fusion neck and answer questions about fundamental timescales in fusion (Riske et al., 2004a; Haluska et al., 2004). In all these applications, the relevant processes taking place, like poration, leakage, pore closure, stretching, and curvature relaxation, appear to exert their influence at different timescales, which it was possible to elucidate with the high temporal resolution achieved with this setup.

APPENDIX A1

Membrane tension and apparent area

The transmembrane potential V_m induces a stress in the bilayer that can be understood in terms of an increase in lateral tension σ_{el} , as expressed by Eq. 3. From the data, in the cases when no macroporation is present, we can calculate the apparent increase in area α_{app} with respect to the vesicle area in the absence of a field (see Eq. 5). As discussed in the text, α_{app} is not the real increase in area α , defined with respect to a tense-free state. Because we do not have access to the initial tension of the vesicle we cannot obtain α from α_{app} . Thus, we are not able to quantitatively correlate the measured increase in α_{app} with the predicted increase in lateral tension σ_{el} with V_m (knowing that $\alpha = \sigma/K$; Needham, 1995). Fig. 7 A shows α_{app} measured for three pulses that did not induce macroporation ($E = 1$ kV/cm, $t_p = 50, 150, 250$ μs , same as in Fig. 1 A). Shown in the right y axis is the induced electrical tension σ_{el} calculated from Eqs. 3 and 1. To estimate σ_{el} after the pulse, a discharging time equal to the charging time (Eq. 2) was used:

$$\sigma_{\text{el}} = \begin{cases} \epsilon\epsilon_0 (h/2h_c^2) \left[1.5 R \cos \theta E (1 - e^{-t/\tau_{\text{charg}}}) \right]^2 & \text{for } t < t_p \\ \epsilon\epsilon_0 (h/2h_c^2) \left[1.5 R \cos \theta E (1 - e^{-t_p/\tau_{\text{charg}}}) e^{-(t-t_p)/\tau_{\text{charg}}} \right]^2 & \text{for } t > t_p \end{cases} \quad (6)$$

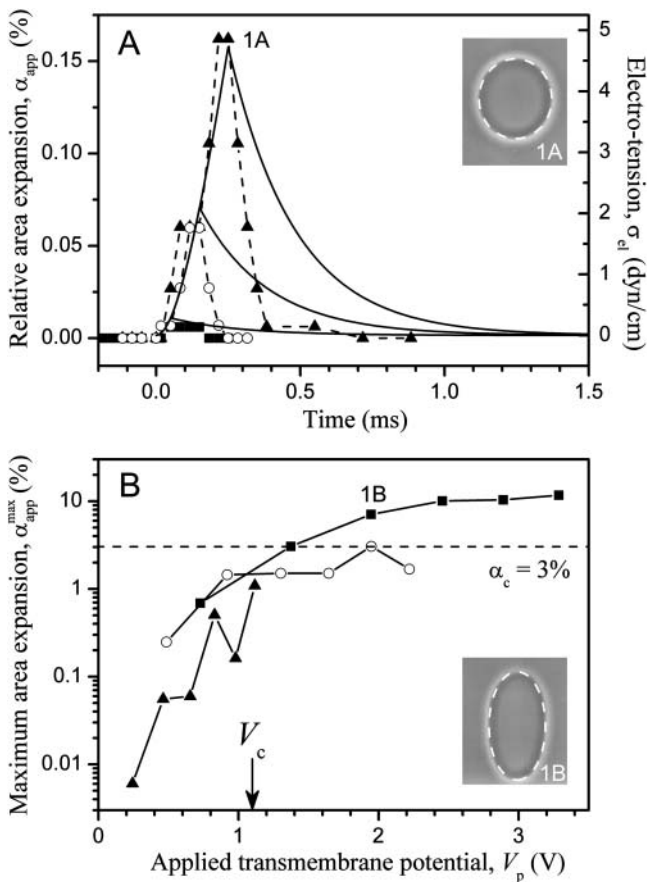


FIGURE 7 (A) Apparent relative area change (α_{app}) calculated from Eq. 5 as a function of time for consecutive pulses: $E = 1$ kV/cm, $t_p = 50$ (\blacksquare), 150 (\circ), and 250 (\blacktriangle) μ s. Time $t = 0$ was set as the beginning of the pulse. The solid lines (right axis) show the electrical tension σ_{el} induced on the membrane calculated for the same three pulses; see Eq. 6. (B) Maximum relative area increase, α_{app}^{max} , for all pulses from the sequence shown in Fig. 1. The data for each pulse strength ($E = 1$ kV/cm, \blacktriangle ; 2 kV/cm, \circ ; and 3 kV/cm, \blacksquare) are shown as a function of the applied transmembrane potential at the end of the pulse V_p . The dashed line indicates $\alpha_c = 3\%$. Note that α_{app} can be different from the real relative area increase α (see text for details). The two snapshots show the vesicle at maximum deformation for the pulses $E = 1$ kV/cm, $t_p = 250$ μ s (1A) and $E = 3$ kV/cm, $t_p = 150$ μ s (1B). The dashed lines are ellipses constructed with the same $(a/b)_{max}$ as experimentally measured.

The two axes were matched to bring the maximum values of α_{app} and σ_{el} together. The snapshots show the vesicle at maximum deformation for the longer pulses. The dashed lines are ellipses with the same a/b ratio, showing that at conditions of no poration the vesicle shape is very close to a perfect ellipsoid. The vesicle response ($t < t_p$) obtained experimentally (data points for α_{app}) and theoretically (calculated curve for σ_{el}) agree quite well. On the other hand, the relaxation dynamics ($t > t_p$) as measured experimentally is slower than theoretically predicted, presumably because this vesicle had some initial tension σ_0 , as discussed in the text (Fig. 2). To check the quantitative agreement between predicted area change and real area change, information on the initial tension of the vesicle should be available.

The analysis discussed above is relevant only for cases when no poration is expected because above the electroporation threshold no volume and area constraint apply. We recall that: i), α_{app} is different from the

relative area increase, α , of a vesicle with zero initial tension and no excess area, and ii), α_{app} might contain contributions from both volume loss and macropore area. The maximum relative area change, α_{app}^{max} , achieved by the vesicle shown in Fig. 1 as a result of each pulse in the sequence is shown in Fig. 7 B. We observe that for the cases when no macroporation occurs, α_{app}^{max} reaches $\sim 0.15\%$ (Fig. 7 A). Actually, the value of α_{app}^{max} for non-macroporated vesicles should be limited from above by 3%, which is reported as the critical maximum stretching, α_c , that lipid bilayers can sustain before they rupture (Needham and Hochmuth, 1989). We see that $\alpha_{app}^{max} > 3\%$ for almost all pulses of the stronger pulse sequence ($E = 3$ kV/cm). This shows that extra area is contributed by the macropores and also that the volume might decrease during the pulse. The fact that macroporation was observed for conditions $\alpha_{app}^{max} < 3\%$, as in $E = 2$ kV/cm (Fig. 1 B), indicates that the vesicle had some initial tension σ_0 , as was already discussed in the text and in Fig. 2. Apart from influencing the relative area increase, macroporation affected the shape of the vesicle. For the stronger pulses the vesicle shape was no longer a perfectly symmetric ellipsoid (see vesicle snapshots), as compared with elliptical shapes with the same a/b ratio (dashed lines).

APPENDIX A2

Comparison with theoretical predictions

We attempted to compare our data on the response and relaxation of the deformation ratio, a/b , with already existing perturbation theories (Hyuga et al., 1991a,b). These two models consider membranes to behave as insulators (i.e., the vesicles do not porate) and as conducting sheets (i.e., vesicles that instantly porate with the applied pulse). In these models, the presence of the electric field induces a stress on the bilayer surface, as given by the Maxwell tensor. The stretching of the membrane, which should be balanced by the tangential component of the electric force, is ignored and the area of the membrane is assumed to remain unchanged. To describe the dynamics of the vesicle deformation Hyuga et al. (1991a,b) performed hydrodynamic calculations where inertial terms are accounted for. Several mysterious parameters of the system, e.g., some “not well-established” mass factor, ν_{mass} , and a resistance factor, γ_{res} , enter the final expressions for a/b . These two parameters, ν_{mass} and γ_{res} , define the inertial and the resistance terms, respectively, in the equation of motion. The authors find that for porated vesicles the deformation depends critically on the conductivity ratio between the external and internal vesicle solutions, $\lambda_{in}/\lambda_{out}$, whereas in the nonporated cases the conductivity ratio is irrelevant.

To compare our results with the theoretical predictions of Hyuga et al. (1991a,b) we consider the two data sets from Fig. 3: a nonmacroporated and a macroporated vesicle. The comparison between the data and the theoretical predictions is presented in Fig. 8. The following parameters were used to construct the theoretical curves. The vesicle radius, $R = 15$ μ m, corresponds to the radius of the experimentally measured vesicles. The resistance factor is chosen to be $\gamma_{res} = 15$ g cm $^{-2}$ s $^{-1}$. Typically, the value that Hyuga et al. (1991a,b) use is 7.5 g cm $^{-2}$ s $^{-1}$, which gives unreasonably high values for a/b compared to our experimental data. If γ_{res} is increased above 15 g cm $^{-2}$ s $^{-1}$ the entire process is slowed down, i.e., shifted in time even further away from the data. The mass factor is chosen to be $\nu_{mass} = 10$, which is the typical value used by Hyuga et al. (1991a,b). The pulse strength and duration correspond to those in the experiments. The conductivity ratio used in the porated case (Fig. 8 B) was $\lambda_{in}/\lambda_{out} = 1.3$. A small deviation in this value, which would correspond to an error in the experimentally measured conductivity ratio, can lead to significant differences from the theoretical curve. In both cases (porated and nonporated), the theoretical curves seem to give a relatively good but, unfortunately, only qualitative description of the process. As in the experiments, the predicted relaxation process for nonporated vesicles is much shorter than for porated ones. For the case where macroporation occurs the plateau-like feature, as mentioned in the discussion of Figs. 1 C and 3 B, is also predicted from the theoretical calculations; see Fig. 8 B (we remind that this feature is overemphasized by

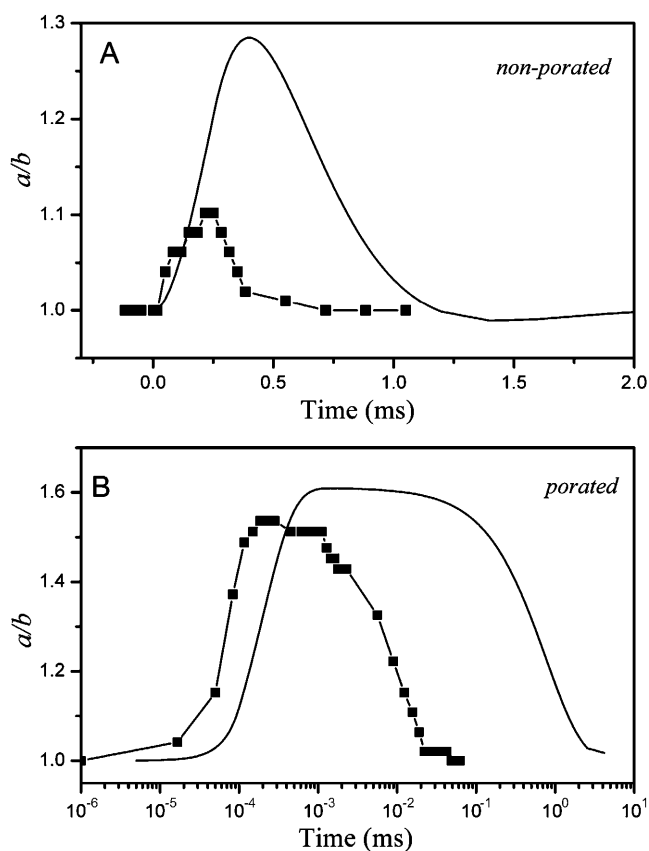


FIGURE 8 Experimental data (■; same as in Fig. 3) and theoretical predictions (solid curves; according to Hyuga et al., 1991a,b) for the response and relaxation dynamics of a vesicle subjected to pulses below (A) and above (B) the poration limit. (A) $E = 1$ kV/cm, $t_p = 250$ μ s ($V_p < V_c$) and (B) $E = 3$ kV/cm, $t_p = 100$ μ s ($V_p > V_c$). The theoretical curves, according to (A) Hyuga et al. (1991b) and (B) Hyuga et al. (1991a), have been calculated for the same pulse strength and duration, vesicle radius ($R = 15$ μ m) as in the experiments, resistance factor $\gamma_{res} = 15$ g cm⁻² s⁻¹ and mass factor $\nu_{mass} = 10$. For the porated case (B), a conductivity ratio $\lambda_{in}/\lambda_{out} = 1.3$ was used (see text for details).

the logarithmic scale). Presumably, it is due to the inertial terms taken into account in the hydrodynamic equations solved in Hyuga et al. (1991a,b).

We did not pursue finding the best set of parameters (γ_{res} , ν , $\lambda_{in}/\lambda_{out}$) because this requires a minimization procedure, which was not the purpose of our work. However, it is clear that using a set of physically reasonable parameters yields a qualitative but not quantitative description of the data.

Attempts to use a more elaborate model where the vesicle is initially an insulator and porates only after a certain time (Hyuga et al., 1991b) also did not lead to better agreement between theory and experiment. We can only conclude that Hyuga et al. (1991a,b) qualitatively predict the experimentally measured values of the deformation ratio a/b . In addition, their model does not account for effects related to vesicles with large excess area (i.e., small reduced volume) where the third relaxation regime characterized by τ_3 was observed.

We thank Antje Reinecke for her technical assistance and help in the data processing. We are also grateful to Reinhard Lipowsky for the support and the suggestions concerning the dimensional analysis. We thank Julian Shillcock for carefully proofreading the text. We acknowledge Dr. D. Dudas for the stimulating discussions and cheerful support.

REFERENCES

- Abidor, I. G., V. B. Arakelyan, L. V. Chernomordik, Y. A. Chizmadzhev, V. F. Pastushenko, and M. R. Tarasevich. 1979. Electric breakdown of bilayer lipid membranes. I. The main experimental facts and their qualitative discussion. *J. Electroanal. Chem.* 104:37–52.
- Angelova, M. I., and D. S. Dimitrov. 1986. Liposome electroformation. *Faraday Discuss. Chem. Soc.* 81:303–311.
- Aranda-Espinoza, H., H. Bermudez, F. S. Bates, and D. E. Discher. 2001. Electromechanical limits of polymersomes. *Phys. Rev. Lett.* 20:208301.
- Bermúdez, H., H. Aranda-Espinoza, D. A. Hammer, and D. E. Discher. 2003. Pore stability and dynamics in polymer membranes. *Europhys. Lett.* 64:550–556.
- Brochard-Wyart, F., P. G. de Gennes, and O. Sandre. 2000. Transient pores in stretched vesicles: role of leak-out. *Physica A.* 278:32–51.
- Cevc, G. 1993. *Phospholipids Handbook*. G. Cevc, editor. Marcel Dekker, New York.
- Chang, D. C., B. M. Chassey, J. A. Saunders, and A. E. Sowers. 1992. *Guide to Electroporation and Electrofusion*. D. C. Chang, B. M. Chassey, J. A. Saunders, and A. E. Sowers, editors. Academic Press, New York.
- Chang, D. C., and T. S. Reese. 1990. Changes in membrane structure induced by electroporation as revealed by rapid-freezing electron microscopy. *Biophys. J.* 58:1–12.
- Chernomordik, L. V., M. M. Kozlov, G. B. Melikyan, I. G. Abidor, V. S. Markin, and Y. A. Chizmadzhev. 1985. The shape of lipid molecules and monolayer membrane fusion. *Biochim. Biophys. Acta.* 812:643–655.
- Chernomordik, L. V., S. I. Sukharev, S. V. Popov, V. F. Pastushenko, A. V. Sokirko, I. G. Abidor, and Y. A. Chizmadzhev. 1987. The electrical breakdown of cell and lipid membranes: the similarity of phenomenologies. *Biochim. Biophys. Acta.* 902:360–373.
- Dimitrov, D. S., and A. E. Sowers. 1990. Membrane electroporation: fast molecular exchange by electroosmosis. *Biochim. Biophys. Acta.* 1022:381–392.
- Dimova, R., C. Dietrich, A. Hadjijsky, K. Danov, and B. Pouligny. 1999. Falling ball viscosimetry of giant vesicle membranes: finite-size effects. *Eur. Phys. J. B.* 12:589–598.
- Dimova, R., U. Seifert, B. Pouligny, S. Förster, and H.-G. Döbereiner. 2002. Hyperviscous diblock copolymer vesicles. *Eur. Phys. J. B.* 7:241–250.
- Discher, B., Y.-Y. Won, D. Ege, J. Lee, F. Bates, D. Discher, and D. Hammer. 1999. Polymersomes: tough vesicles made from diblock copolymers. *Science.* 284:1143–1146.
- Evans, E., V. Heinrich, F. Ludwig, and W. Rawicz. 2003. Dynamic tension spectroscopy and strength of biomembranes. *Biophys. J.* 85:2342–2350.
- Evans, E., and W. Rawicz. 1990. Entropy-driven tension and bending elasticity in condensed-fluid membranes. *Phys. Rev. Lett.* 17:2094–2097.
- Glaser, R. W., S. L. Leikin, L. V. Chernomordik, V. F. Pastushenko, and A. I. Sokirko. 1988. Reversible electrical breakdown of lipid bilayers: formation and evolution of pores. *Biochim. Biophys. Acta.* 940:275–287.
- Griese, T., S. Kakorin, and E. Neumann. 2002. Conductometric and electrooptic relaxation spectrometry of lipid vesicle electroporation at high fields. *Phys. Chem. Chem. Phys.* 4:1217–1227.
- Haluska, C., V. Marchi-Artzner, J. Brienne, J.-M. Lehn, R. Lipowsky, and R. Dimova. 2004. Fusion of giant vesicles observed with time resolution below a millisecond. *Biophys. J.* 86:519a.
- Harbich, W., and W. Helfrich. 1979. Alignment and opening of giant lecithin vesicles by electric fields. *Z. Naturforsch.* 34a:1063–1065.
- Hibino, M., M. Shigemori, H. Itoh, K. Nagayama, and K. Kinoshita, Jr. 1991. Membrane conductance of an electroporated cell analyzed by submicrosecond imaging of transmembrane potential. *Biophys. J.* 59:209–220.
- Hyuga, H., K. Kinoshita, Jr., and N. Wakabayashi. 1991a. Deformation of vesicles under the influence of strong electric fields. *Jpn. J. Appl. Phys.* 30:1141–1148.

- Hyuga, H., K. Kinoshita, Jr., and N. Wakabayashi. 1991b. Deformation of vesicles under the influence of strong electric fields II. *Jpn. J. Appl. Phys.* 30:1333–1335.
- Hyuga, H., K. Kinoshita, Jr., and N. Wakabayashi. 1993. Steady-state deformation of vesicle in alternating fields. *Bioelectrochem. Bioenerg.* 32:15–25.
- Isambert, H. 1998. Understanding the electroporation of cells and artificial bilayer membranes. *Phys. Rev. Lett.* 80:3404–3407.
- Kakorin, S., T. Liese, and E. Neumann. 2003. Membrane curvature and high-field electroporation of lipid bilayer vesicles. *J. Phys. Chem. B.* 107:10243–10251.
- Kakorin, S., and E. Neumann. 2002. Electrooptical relaxation spectroscopy of membrane electroporation in lipids vesicles. *Colloids Surf. A.* 209:147–165.
- Karatekin, E., O. Sandre, H. Guitoni, N. Borghi, P.-H. Puech, and F. Brochard-Wyart. 2003. Cascade of transient pores in giant vesicles: line tension and transport. *Biophys. J.* 84:1734–1749.
- Kinoshita, K., Jr., I. Ashikawa, N. Saita, H. Yoshimura, H. Itoh, K. Nagayama, and A. Ikegami. 1988. Electroporation of cell membrane visualized under a pulsed-laser fluorescence microscope. *Biophys. J.* 53:1015–1019.
- Kinoshita, K., Jr., and T. Y. Tsong. 1977. Voltage-induced pore formation and hemolysis of human erythrocytes. *Biochim. Biophys. Acta.* 471:227–242.
- Kummrow, M., and W. Helfrich. 1991. Deformation of giant lipid vesicles by electric fields. *Phys. Rev. A.* 44:8356–8360.
- Moroz, J. D., and P. Nelson. 1997. Dynamically stabilized pores in bilayer membranes. *Biophys. J.* 72:2211–2216.
- Mutz, M., and H. Helfrich. 1990. Bending rigidities of some biological model membranes as obtained from Fourier analysis of contour sections. *J. Phys. France.* 51:991–1002.
- Needham, D. 1995. Cohesion and permeability of lipid bilayer vesicles. In *Permeability and Stability of Lipid Bilayers*. E. A. Disalvo and S. A. Simon, editors. CRC Press, Boca Raton, FL. 49–76.
- Needham, D., and R. M. Hochmuth. 1989. Electro-mechanical permeabilization of lipid vesicles. Role of membrane tension and compressibility. *Biophys. J.* 55:1001–1009.
- Neumann, E., S. Kakorin, and K. Toensing. 1998. Membrane electroporation and electromechanical deformation of vesicles and cells. *Faraday Discuss.* 111:111–125.
- Neumann, E., A. Sowers, and C. Jordan, editors. 1989. *Electroporation and Electrofusion in Cell Biology*. Plenum, New York.
- Orädd, G., G. Wikander, G. Lindblom, and L. B.-Å. Johansson. 1994. Effect of glycerol on the translational and rotational motions in lipid bilayers studied by pulsed-field gradient ^1H NMR, EPR and time-resolved fluorescence spectroscopy. *J. Chem. Soc. Faraday Trans.* 90:305–309.
- Ramos, C., and J. Teissie. 2000. Electrofusion: a biophysical modification of cell membrane and a mechanism in exocytosis. *Biochimie.* 82:511–518.
- Rawicz, W., K. C. Olbrich, T. McIntosh, D. Needham, and E. Evans. 2000. Effect of chain length and unsaturation on elasticity of lipid bilayers. *Biophys. J.* 79:328–339.
- Riske, K. A., L. Q. Amaral, H.-G. Döbereiner, and M. T. Lamy. 2004b. Mesoscopic structure in the chain-melting regime of anionic phospholipid vesicles: DMPG. *Biophys. J.* 86:3722–3733.
- Riske, K., R. Lipowsky, and R. Dimova. 2004a. High temporal resolution of electro-poration, fusion and deformation of giant vesicles. “Squaring” the vesicles. *Biophys. J.* 86:518a.
- Saitoh, A., K. Takiguchi, Y. Tanaka, and H. Hotani. 1998. Opening-up of liposomal membranes by talin. *Proc. Natl. Acad. Sci. USA.* 95:1026–1031.
- Sandre, O., L. Moreaux, and F. Brochard-Wyart. 1999. Dynamics of transient pores in stretched vesicles. *Proc. Natl. Acad. Sci. USA.* 96:10591–10596.
- Schneider, M. B., J. T. Jenkins, and W. W. Web. 1984. Thermal fluctuations of large cylindrical phospholipid vesicles. *Biophys. J.* 45:891–899.
- Simon, S. A., and T. J. McIntosh. 1986. Depth of water penetration into bilayers. *Methods Enzymol.* 127:511–521.
- Smith, K. C., J. C. Neu, and W. Krassowska. 2004. Model of creation and evolution of stable electropores for DNA delivery. *Biophys. J.* 86:2813–2826.
- Sowers, A. E. 1986. A long-lived fusogenic state is induced in erythrocyte ghosts by electric pulses. *J. Cell Biol.* 102:1358–1362.
- Teissie, J., and T. Y. Tsong. 1981. Electric field induced transient pores in phospholipid bilayer vesicles. *Biochemistry.* 20:1548–1554.
- Tekle, E., R. D. Astumian, and P. B. Chock. 1994. Selective and asymmetric molecular transport across electroporated cell membranes. *Proc. Natl. Acad. Sci. USA.* 91:11512–11516.
- Tekle, E., R. D. Astumian, W. A. Friauf, and P. B. Chock. 2001. Asymmetric pore distribution and loss of membrane lipid in electroporated DOPC vesicles. *Biophys. J.* 81:960–968.
- Weaver, J. C., and Y. A. Chizmadzhev. 1996. Theory of electroporation: a review. *Bioelectrochem. Bioenerg.* 41:135–160.
- Zhelev, D. V., and D. Needham. 1993. Tension-stabilized pores in giant vesicles: determination of pore size and pore line tension. *Biochim. Biophys. Acta.* 1147:89–104.
- Zimmermann, U., and G. A. Neil, editors. 1996. *Electromanipulation of cells*. CRC Press, Boca Raton, FL.